Radiation Measurements 110 (2018) 1–6

Contents lists available at ScienceDirect

Radiation Measurements

journal homepage: www.elsevier.com/locate/radmeas

Theoretical calculation and measurement accuracy of Cerenkov optic-fiber dosimeter under electron and photon radiation therapies

Xudong Zhang[a], Xiaobin Tang[a,b,*], Diyun Shu[a], Chunhui Gong[a], Changran Geng[a,b], Yao Ai[a], Haiyan Yu[a], Wencheng Shao[a]

[a] Department of Nuclear Science and Engineering, Nanjing University of Aeronautics and Astronautics, Nanjing, 210016, China
[b] Collaborative Innovation Center of Radiation Medicine of Jiangsu Higher Education Institutions, Nanjing, 210016, China

ARTICLE INFO

Keywords:
Cerenkov optic-fiber dosimeter
Radiotherapy
Response difference
Measurement accuracy

ABSTRACT

This work aimed to study the mechanism and understand the influencing factors of measurement accuracy for the Cerenkov optic-fiber dosimeter under electron and photon radiation therapies. Through the Geant4 calculation, we determined responses between Cerenkov photon numbers recorded by the measurement device and the dose deposited in the fiber and found responses differed for electron and photon beam irradiations. For electron beams, the relative Cerenkov photon number recorded by the device agreed well with the relative dose for the depths after the maximum dose depth, but differed before that depth. For the photon beams, the relative Cerenkov photon number showed good agreement with the relative dose for all depths. Considering the transmission efficiency of the Cerenkov radiation in the fiber, energy spectra and angular distributions of electrons were analyzed to explain the response difference. For the photon beams, energy spectra and angular distributions of electrons changed less in various phantom depth than electron beams, therefore, better response was observed for photon beams. Besides, the influences of fiber parameters (i.e. diameter, refractive index, and material) were investigated. With the increase of the core diameter, the transmission efficiency of Cerenkov radiation changed slightly but the Cerenkov photon numbers produced in the fiber increased by square. With smaller ratio of cladding/core refractive index or using PMMA as the core materials, Cerenkov photon numbers recorded by the device could also be increased. This study could provide better understanding of the Cerenkov optic-fiber dosimeter and promote its development.

1. Introduction

Dose measurement technology in advanced radiotherapy is important to ensure the accuracy of dose delivery and is an effective method of quality assurance and control. Although the ionization chamber and thermoluminescence dosimeter have been available for commercial application, certain problems still exist in dose measurements for radiotherapy (Kron et al., 1996; Stenstrom and Marvin, 1946). The scintillating fiber-optic dosimeter (SFOD) is recently developed with several advantages, such as good tissue equivalence, high spatial resolution, and remote measurement capability. However, the quenching effect of scintillator and the Cerenkov light noise limit the use of SFOD in clinical situations (Mouatassim et al., 1995). In recent years, researchers have suggested the new Cerenkov optic-fiber dosimeter (CFOD), which removes the scintillator of the SFOD and directly detects the Cerenkov radiation to characterize the radiation dose (Jang et al., 2012, 2013; Lee et al., 2013; Yoo et al., 2013a, 2013b).

Cerenkov radiation is an electromagnetic radiation produced by a charged particle traveling through a transparent medium at a velocity greater than that of light in the same medium (Beddar et al., 1992). Although fluorescence photons and Cerenkov photons can be both generated during x-ray and electron irradiation, light generated in the optical fiber were mostly composed of light from the Cerenkov effect (94%–100% contribution) for high-energy modalities (e.g. radiation therapy) (Therriault-Proulx et al., 2013). As a light signal generated in the dosimeter through radiation interaction, Cerenkov radiation has a certain relationship with the energy deposition of particles and has the potential to be used for dose measurement (Shu et al., 2016a, 2016b). … The CFOD uses the Cerenkov radiation generated in the fiber to characterize the dose by Cerenkov light intensity, as shown in Fig. 1. Researchers (Jang et al., 2013; Yoo et al., 2013b) carried out considerable experimental verification of the CFOD under different radiations, such as electron and photon radiations. They have demonstrated the potential and viability of the dosimeter for radiotherapy dose

* Corresponding author. Department of Nuclear Science and Engineering, Nanjing University of Aeronautics and Astronautics, Nanjing, 210016, China.
E-mail address: tangxiaobin@nuaa.edu.cn (X. Tang).

https://doi.org/10.1016/j.radmeas.2018.01.001
Received 27 May 2017; Received in revised form 19 October 2017; Accepted 13 January 2018
Available online 31 January 2018
1350-4487/

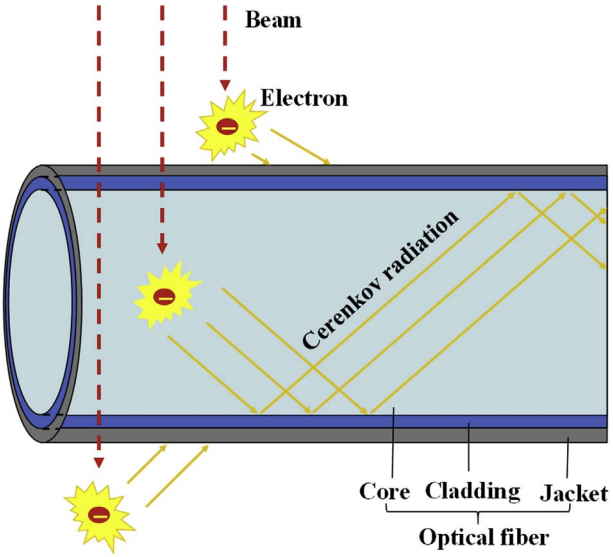

Fig. 1. Measurement diagram of the Cerenkov optic-fiber dosimeter.

measurement.

Although much verification has been conducted, the intrinsic physical mechanism of the CFOD and the factors that affect the dose measurement still need to be further studied. Using the Monte Carlo toolkit Geant4, a CFOD model and the radiation transportation process were simulated (Agostinelli et al., 2003). The relationships between the Cerenkov photon numbers (CPNs) and the deposited dose were analyzed. The intrinsic physical mechanism of the dosimeter was studied. The influences of fiber parameters, such as core diameter, ratio of cladding/core refractive index, and core material, on measurement were investigated, thereby providing a basis for improving the dose measurement accuracy.

2. Materials and methods

Geant4 is a public toolkit which can be used to accurately simulate the passage of particles through matter. A three-dimensional water phantom and a CFOD model were constructed in Geant4 (version 10.01.p02), as shown in Fig. 2. The size of the phantom was 25 cm × 25 cm × 25 cm. Step-index plastic optical fibers were used to generate and transmit Cerenkov radiation with a core/cladding structure. The outer diameter of the plastic optical fiber was 1.0 mm, and the thickness of cladding was 0.01 mm. The refractive indices of the core and the cladding were 1.492 and 1.402, respectively. The materials of the core and the cladding were polymethyl methacrylate (PMMA) and fluorinated polymer, respectively. The fiber was covered by a polyethylene (PE)-based black jacket to intercept external light noise (Yoo et al., 2013b).

Generally, the subtraction method can be used to measure the signal difference of two fibers (Clift et al., 2002). To apply the subtraction method, two fibers with different lengths were placed closely and the length difference L was considered the measurement region. CPNs recorded by the device were obtained by subtracting the signal of the shorter fiber at the measurement device from the longer one. The deposited dose and the CPNs generated in the fiber were directly obtained through Geant4 simulation.

When the beam irradiated on the fibers, the Cerenkov radiation generated in the fibers was transmitted to the measurement device through a long optical fiber. For remote measurement, the fiber had a length of 25 m between the measurement device and the phantom. The energy spectra and the angular distributions of electrons at different depths of phantom were also calculated.

Electron and photon beams are commonly used in radiotherapy. The two beams with energies of 6, 9, and 15 MeV were simulated in the current study. All beams we used were set to be non-clinical monoenergetic to study the mechanism under relatively simplified conditions. The field size of the planer source was maintained at 10 cm × 10 cm. The distance between the source and the phantom surface was 80 cm. The beams perpendicularly irradiated the phantom along the central axis. Therefore, the size of irradiation field was the same as that of the source.

3. Results and discussion

3.1. Relationship between CPNs and dose

It was necessary to determine the length difference of two fibers first. Fig. 3 illustrates the relationship between CPNs generated in the fiber per irradiated particle and the length difference of two fibers. The CPNs are linearly correlated to the length difference. When the length difference is small, the spatial resolution of dose measurement is high, thereby resulting in less CPNs produced in the fiber. A balance exists between the precision and accuracy of dose measurement in terms of the length difference. After comprehensive consideration, the length difference was set to 10 mm.

Fig. 4 shows the generated and detected CPNs curves and the percent depth dose (PDD) curves under the electron beam at irradiation energies of 6, 9, and 15 MeV. The two CPNs curves were normalized to their largest values and compared with the PDD curve deposited in the fiber. The CPNs curves generated in the fiber agree well with the PDD

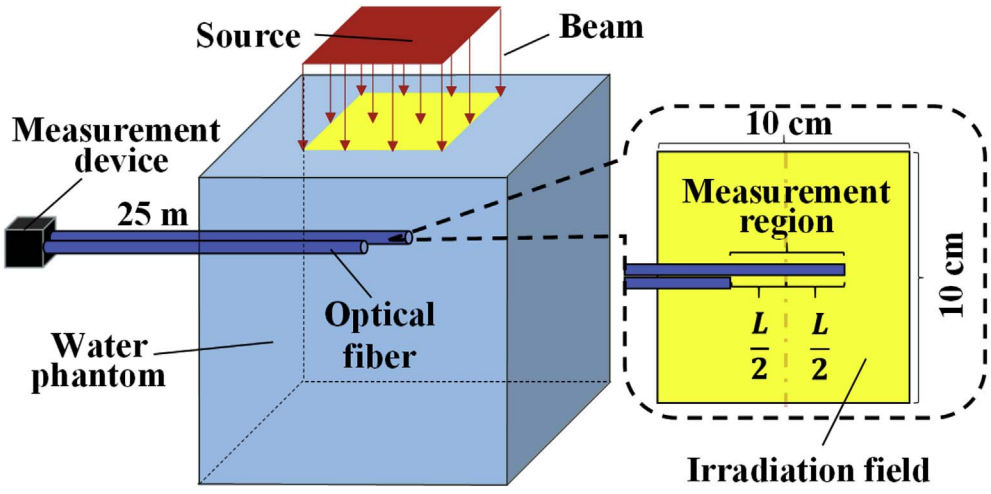

Fig. 2. Schematic of calculation model.

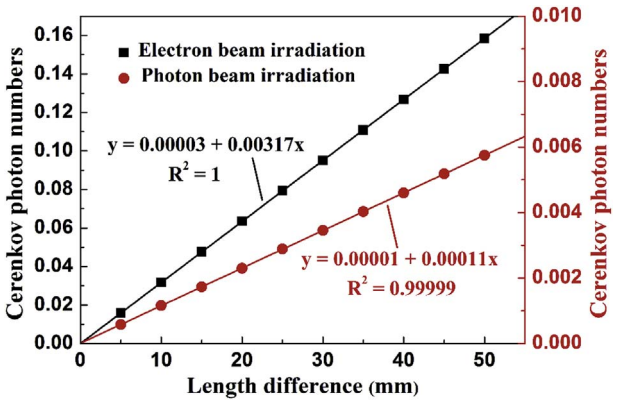

Fig. 3. Relationship between Cerenkov photon numbers generated in the fiber per irradiated particle and the length difference of two fibers.

curves. However, the CPNs curves recorded by the device differ first from the PDD curves before the maximum dose depth and then become similar after that depth. On this basis, the CPNs curve recorded by the measurement device may only be used to characterize the dose distribution after the maximum dose depth without additional corrections for electron beam irradiations. This result is consistent with the experiment of Yoo on electron beams (Yoo et al., 2013b).

Fig. 5 shows the generated and detected CPNs curves and the PDD curves under the photon beam at irradiation energies of 6, 9, and 15 MeV. The two CPNs curves were also normalized to their largest values. The CPNs curves generated in the fiber shows a good relationship with the dose curves deposited in the fiber. The CPNs curves recorded by the device present some deviations with the two other curves, but these deviations are within the acceptable range. Therefore, for irradiations of photon beams, the CPNs curve recorded by the measurement device can be used to characterize the dose distribution for all depths of phantom.

3.2. Mechanism study of the CFOD

The CPNs generated in the fiber agree well with the dose deposited in the fiber for the two beam irradiations. Nevertheless, responses between CPNs recorded by the device and the dose deposited in the fiber differ for the electron and photon beam irradiations. The response difference is attributed to the transmission of the Cerenkov radiation in the fiber. The transmission efficiency (TE) of the Cerenkov radiation can be defined as the ratio of CPNs recorded by the measurement device to CPNs generated in the fiber, as follows:

$$\mathrm{TE} = \frac{\text{CPNs recorded by the measurement device}}{\text{CPNs generated in the fiber}} \quad (1)$$

The response difference under the electron and photon beam irradiations is attributed to the different TEs of the Cerenkov radiation in fibers at different depths of phantom.

Considering that the Cerenkov radiation is produced from electrons for photon and electron beam irradiations, the energy spectrum and the angular distribution of electrons were analyzed to learn the mechanism of the response difference. Electron energy determined the emission direction of the Cerenkov radiation, which is related to the total reflection of the Cerenkov radiation in the fiber. The angle between the electron orientation and fiber axis also matters in the total reflection (Mei et al., 2006). Different energy spectra and angular distributions of electrons at different depths of phantom can affect the TEs, thereby resulting in the response difference. Hence, the electron energy spectrum and the electron angular distribution were analyzed.

Fig. 6(a) and (b) show the normalized electron energy spectra at different depths of phantom irradiated by electron and photon beams at 9 MeV, respectively. Every spectrum was normalized to its largest

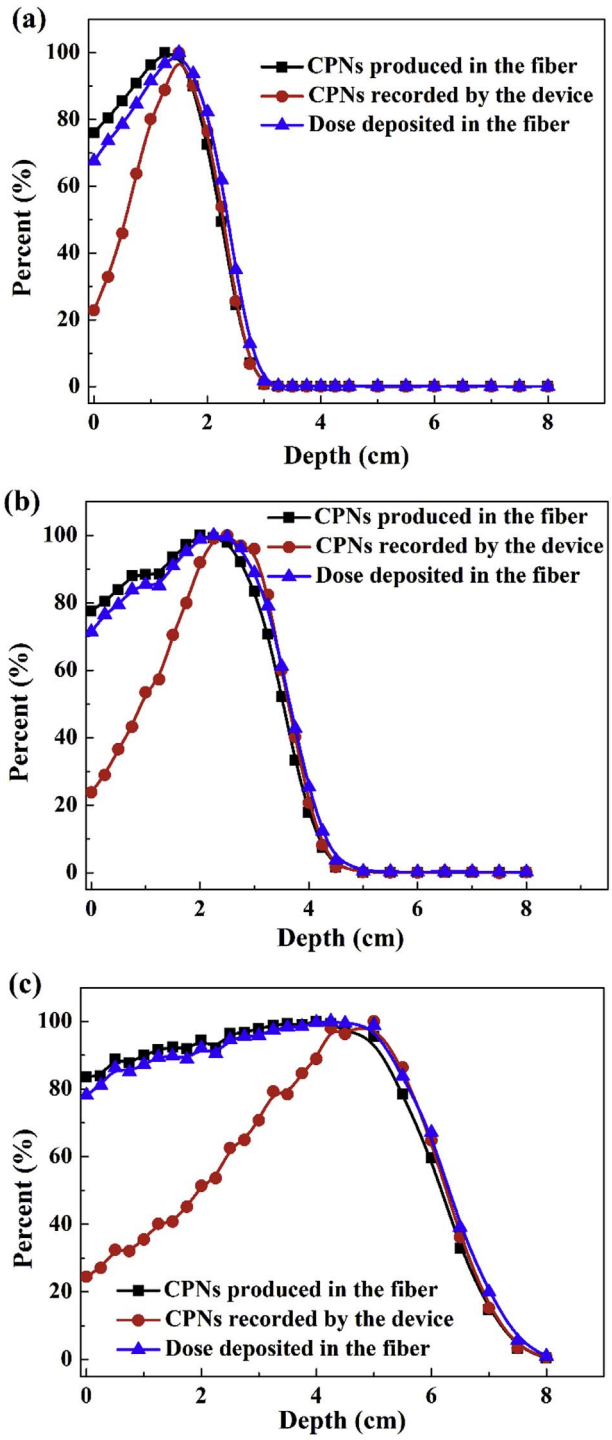

Fig. 4. CPNs and PDD curves as a function of the depths of phantom under the electron beam at irradiation energies of (a) 6, (b) 9, and (c) 15 MeV.

value. Several depths were selected depending on the irradiation range of the beam. At the shallow depth, high-energy and low-energy components are found in the electron energy spectrum. The maximum energy of electrons is close to the energy of incident particle. With the increase in the depth, the high-energy electrons are transformed to low-energy electrons until the high-energy component disappears. Different electron energy spectra result in different TEs of the Cerenkov radiation at different depths of phantom. Compared with electron beam irradiations, the change in electron energy spectra with the increase in depth under photon beam irradiations is smaller. Thus, the response between CPNs recorded by the device and the dose deposited in the fiber is

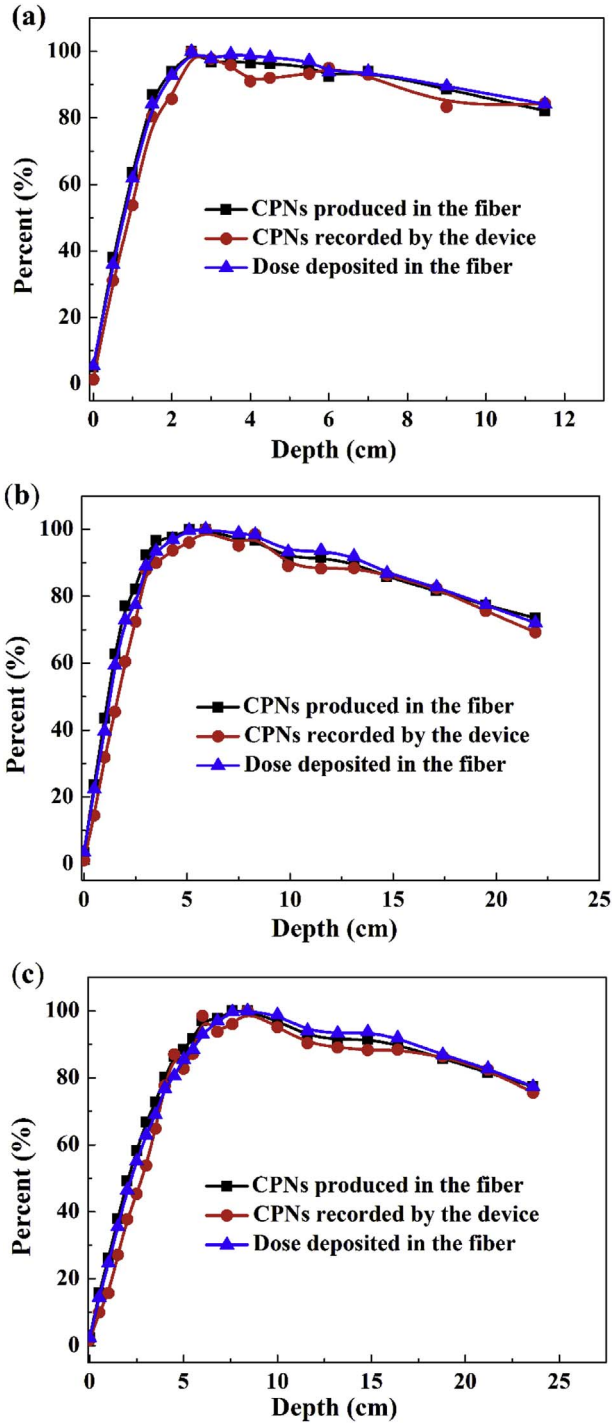

Fig. 5. CPNs and PDD curves as a function of the depths of phantom under the photon beam at irradiation energies of (a) 6, (b) 9, and (c) 15 MeV.

better under photon beam irradiations than under electron beam irradiations.

Fig. 7(a) and (b) show the angular distributions of electrons at different depths of phantom under the electron and photon beam irradiations at 9 MeV, respectively. The angular distributions of electrons were obtained at the same depths where the energy spectra were recorded. Angles of electrons concentrate at 90° at the shallow depth, and the peak broadens with the increase in depth. After a certain depth, the angular distribution stabilizes. Different angular distributions of electrons also result in different TEs of the Cerenkov radiation. Compared with those under photon beam irradiations, the angular distributions

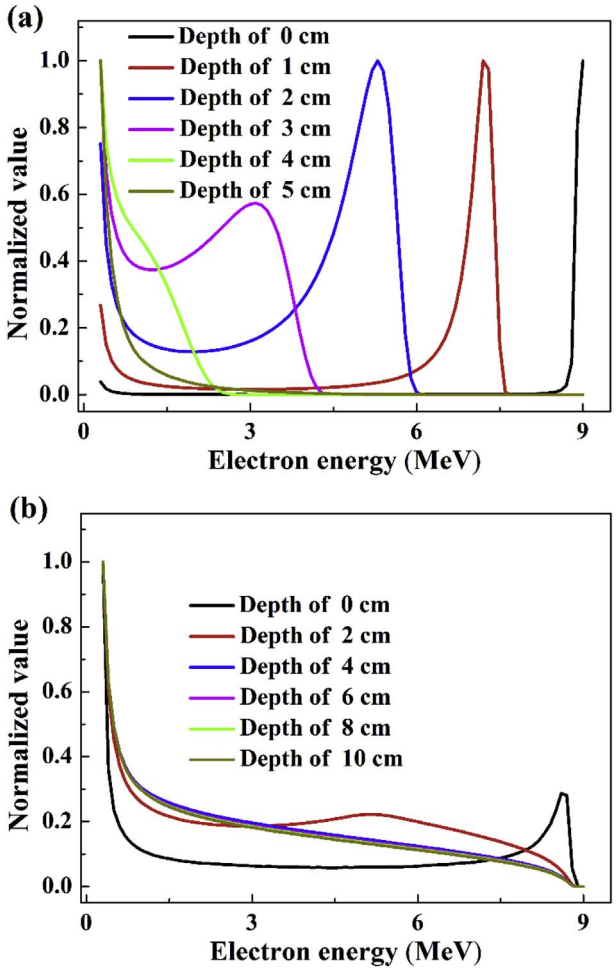

Fig. 6. Normalized electron energy spectra at different depths of phantom irradiated by (a) electron beam and (b) photon beam.

under the electron beam irradiations change more significantly with the increase in depth, thereby resulting in a worse response between the CPNs recorded by the measurement device and the dose deposited in the fiber.

3.3. Influence of fiber parameters on the measurement accuracy

According to the statistics principle, the more CPNs recorded by the measurement device are, the more accurate the measurement result is. Equation (1) shows that the measurement accuracy can be improved by increasing the CPNs generated in the fiber or increasing TEs. Given that the two methods are related to fiber parameters, the influences of fiber parameters on the measurement accuracy were studied. The core diameter, the ratio of cladding/core refractive index and the core material of the fiber were discussed under electron and photon beams at 9 MeV.

The plastic optical fibers were placed at different depths of phantom, which were selected according to the irradiation range of the beam. The thicknesses of the cladding and jacket were kept constant and only the core diameter was changed. Fig. 8 shows the TEs of the Cerenkov radiation as a function of the core diameter at different depths. The TEs slightly change with the increase in the core diameter at the same depth. Laws are identical under electron and photon beam irradiations and do not vary with the depths. Therefore, the core diameter of fibers has no effect on the TEs of the Cerenkov radiation. Fig. 9 illustrates the CPNs generated in the fiber as a function of the core diameter when the fibers were placed at the maximum dose depth of the beam. In our simulation, CPNs generated in the fiber are

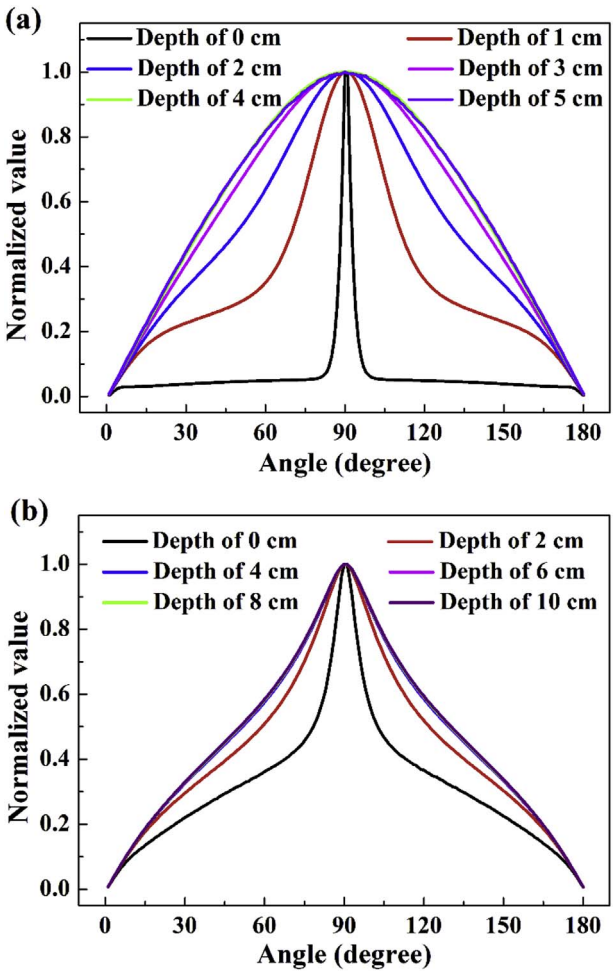

Fig. 7. Angular distributions of electrons at different depths of phantom irradiated by (a) electron beam and (b) photon beam.

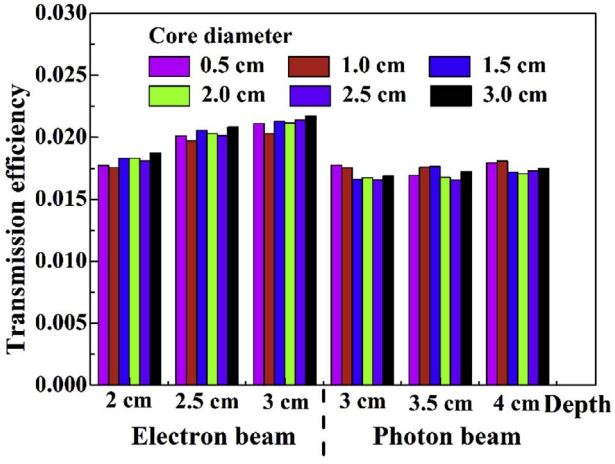

Fig. 8. Transmission efficiency as a function of the core diameter at different depths.

proportional to the square of the core diameter.

The length difference of two fibers determined earlier can achieve good spatial resolution in dose measurement but may not be excellent for statistics. This problem can be addressed by increasing the core diameter. Meanwhile, the spatial resolution of measurement in the radial direction of fiber decreases inevitably with the increase in the core diameter. For practical applications, the accuracy and spatial resolution of dose measurement should be considered simultaneously.

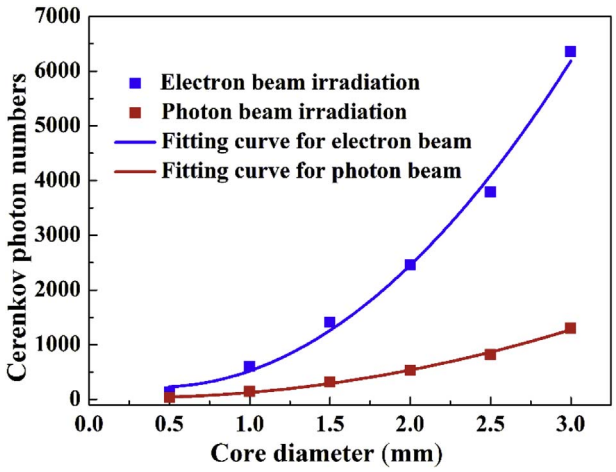

Fig. 9. CPNs generated in the fiber as a function of the core diameter.

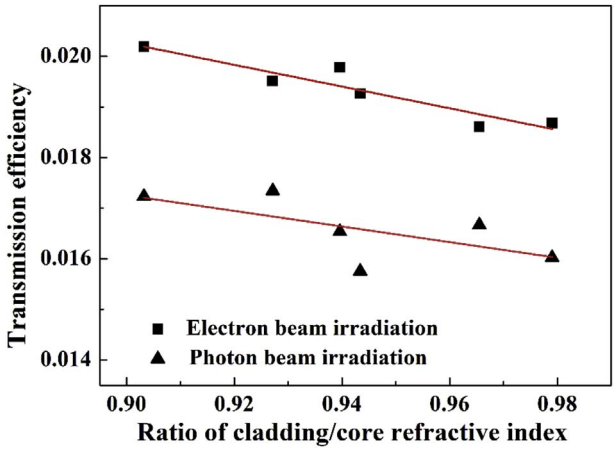

Fig. 10. Transmission efficiency as a function of the ratio of cladding/core refractive index.

According to the refractive index range of frequently-used fiber materials (approximately 1.4–1.6), the ratio of cladding/core refractive index was changed and TEs of the Cerenkov radiation in fibers were obtained. Fig. 10 shows the TEs as a function of the ratio of cladding/core refractive index at the maximum dose depth of the beam. The TEs decrease with the increase in the ratio for both beam irradiations. The fiber with a small ratio of cladding/core refractive index is conducive to transmitting the Cerenkov radiation, which should be considered for choosing fibers.

The propagation attenuation of the Cerenkov radiation in fibers was determined by the core material. Thus, the effect of different core materials on the TEs should be investigated. For common core materials, such as PMMA, polycarbonate (PC), and polystyrene (PS), Table 1 shows the TEs of the Cerenkov radiation in the three fibers with three kinds of core materials under two beam irradiations (Polishuk, 2006). The TE of the Cerenkov radiation in the fiber with PMMA core material

Table 1
TEs of the Cerenkov radiation in three fibers with different core materials.

Beam	No. of fiber	Core material	Transmission efficiency
Electron	1	PMMA	0.01933
Electron	2	PC	0.00002
Electron	3	PS	0.00651
Photon	1	PMMA	0.01703
Photon	2	PC	0.00002
Photon	3	PS	0.00518

is largest among the three fibers with different core materials. PMMA material is suitable to be used as the core material of the fiber for transmitting the Cerenkov radiation.

4. Conclusion

In this study, a CFOD model and a water phantom were constructed using the Monte Carlo toolkit Geant4. Irradiations of electron and photon beams were simulated. The CPNs recorded by the measurement device, the CPNs generated in the fiber, and the dose deposited in the fiber were analyzed.

For the irradiations of electron or photon beams, the CPNs generated in the fiber present a certain response relationship with the dose deposited in the fiber. However, responses between the CPNS recorded by the device and the dose deposited in the fiber differ for electron and photon beam irradiations. Characterizing the dose by CPNs recorded by the device is useful for all depths under photon beam irradiations, but useful only after the maximum dose depth under electron beam irradiations. The energy spectra and the angular distributions of electrons were analyzed and various degrees of change of the two aspects with the increase in depth under the two beam irradiations are the main reasons for the response difference. The influences of fiber parameters, such as core diameter, ratio of cladding/core refractive index, and core material, on the CPNs recorded by the measurement device were discussed. These fiber parameters influence the dose measurement accuracy and are essential in selecting the appropriate parameters based on actual needs. The study can provide better understanding of and promote the research on the Cerenkov optic-fiber dosimeter.

Acknowledgments

This work was supported by the National Natural Science Foundation of China [Grant No. 11475087]; the National Key Research and Development Program [Grant No. 2016YFE0103600]; the National Key Research and Development Program (Grant No. 2017YFC0107700); the Foundation of Graduate Innovation Center in NUAA (Grant No. kfjj20170617) and the Priority Academic Program Development of Jiangsu Higher Education Institutions.

References

Agostinelli, S., Allison, J., Amako, K., Apostolakis, J., Araujo, H., Asai, M., Axen, D., Banerjee, S., Barrand, G., Behner, F., et al., 2003. GEANT4—a simulation toolkit. Nucl. Instrum. Meth. Phys. Res. A 506, 250–303. http://doi.org/10.1016/S0168-9002(03)01368-8.

Beddar, A.S., Mackie, T.R., Attix, F.H., 1992. Cerenkov light generated in optical fibres and other light pipes irradiated by electron beams. Phys. Med. Biol. 37, 925.

Clift, M.A., Johnston, P.N., Webb, D.V., 2002. A temporal method of avoiding the Cerenkov radiation generated in organic scintillator dosimeters by pulsed mega-voltage electron and photon beams. Phys. Med. Biol. 47, 1421. http://dx.doi.org/10.1088/0031-9155/47/8/313.

Jang, K.W., Yagi, T., Pyeon, C.H., Yoo, W.J., Shin, S.H., Jeong, C., Min, B.J., Shin, D., Misawa, T., Lee, B., 2013. Application of Cerenkov radiation generated in plastic optical fibers for therapeutic photon beam dosimetry. J. Biomed. Optic. 18, 027001. https://doi.org/10.1117/1.JBO.18.2.027001.

Jang, K.W., Yoo, W.J., Shin, S.H., Shin, D., Lee, B., 2012. Fiber-optic Cerenkov radiation sensor for proton therapy dosimetry. Optic Express 20, 13907–13914. https://doi.org/10.1364/OE.20.013907.

Kron, T., Butson, M., Hunt, F., Denham, J., 1996. TLD extrapolation for skin dose determination in vivo. Radiother. Oncol. 41, 119–123. https://doi.org/10.1016/S0167-8140(96)01795-1.

Lee, B., Jang, K.W., Yoo, W.J., Shin, S.H., Moon, J., Han, K.T., Jeon, D., 2013. Measurements of Cerenkov lights using optical fibers. IEEE Trans. Nucl. Sci. 60, 932–936. http://dx.doi.org/10.1109/TNS.2013.2252623.

Mei, X., Rowlands, J.A., Pang, G., 2006. Electronic portal imaging based on Cerenkov radiation: a new approach and its feasibility. Med. Phys. 33, 4258–4270. http://dx.doi.org/10.1118/1.2362875.

Mouatassim, S., Costa, G.J., Guillaume, G., Heusch, B., Huck, A., Moszyński, M., 1995. The light yield response of NE213 organic scintillators to charged particles resulting from neutron interactions. Nucl. Instrum. Meth. Phys. Res. A 359, 530–536. https://doi.org/10.1016/0168-9002(95)00020-8.

Polishuk, P., 2006. Plastic optical fibers branch out. IEEE Commun. Mag. 44, 140–148. http://dx.doi.org/10.1109/MCOM.2006.1705991.

Shu, D., Tang, X., Geng, C., Gong, C., Chen, D., 2016a. Determination of the relationship between dose deposition and Cerenkov photons in homogeneous and heterogeneous phantoms during radiotherapy using Monte Carlo method. J. Radioanal. Nucl. Chem. 308, 187–193. http://dx.doi.org/10.1007/s10967-015-4316-x.

Shu, D., Tang, X., Guan, F., Geng, C., Yu, H., Gong, C., Zhang, X., Chen, D., 2016b. Analysis of the relationship between neutron dose and Cerenkov photons under neutron irradiation through Monte Carlo method. Radiat. Meas. 93, 35–40. http://doi.org/10.1016/j.radmeas.2016.07.001.

Stenstrom, K.W., Marvin, J.F., 1946. Ionization measurements with bone chambers and their application to radiation therapy. Am. J. Roentgenol. 56, 759–770.

Therriault-Proulx, F., Beaulieu, L., Archambault, L., Beddar, S., 2013. On the nature of the light produced within PMMA optical light guides in scintillation fiber-optic dosimetry. Phys. Med. Biol. 58, 2073–2084. http://dx.doi.org/10.1088/0031-9155/58/7/2073.

Yoo, W.J., Han, K.T., Shin, S.H., Seo, J.K., Jeon, D., Lee, B., 2013a. Development of a Cerenkov radiation sensor to detect low-energy beta-particles. Appl. Radiat. Isot. 81, 196–200. http://doi.org/10.1016/j.apradiso.2013.03.075.

Yoo, W.J., Shin, S.H., Jeon, D., Hong, S., Kim, S.G., Sim, H.I., Jang, K.W., Cho, S., Lee, B., 2013b. Simultaneous measurements of pure scintillation and Cerenkov signals in an integrated fiber-optic dosimeter for electron beam therapy dosimetry. Optic Express 21, 27770–27779. https://doi.org/10.1364/OE.21.027770.